# Meso-aryl substituents modify the electrochemical profile and palladium(II) coordination of redox-active tripyrrin ligands

Iva Habenšus and Elisa Tomat\*

The tripyrrin coordination motif, namely a conjugated tripyrrolic fragment of the porphyrin scaffold, is found in numerous metal complexes of oligopyrrolic macrocycles. Because of their typically limited stability, linear tripyrrins are underutilized in coordination chemistry; however, hexaalkyl-tripyrrindiones featuring the pyrrolinone termini characteristic of biopyrrin pigments have recently emerged as versatile redox-active ligands. Herein, we report the synthesis of the first example *meso*-di(pentafluorophenyl) tripyrrin-1,14-dione ligand through the demethylation of a stable 1,14-dimethoxytripyrrin precursor. The two tripyrrin ligands coordinate palladium(II) in square planar geometries in completely distinct ways: the dimethoxytripyrrin forms a cyclopalladate following  $C(sp^3)$ —H bond activation at one of the methoxy groups, whereas the tripyrrindione binds as a trianionic ligand engaging an adventitious aqua ligand in hydrogen-bonding interactions. When compared to the hexaalkyl-tripyrrindiones, the *meso*-aryl substituents significantly alter the electrochemical profile of the Pd(II) tripyrrindione complex, shifting anodically by ~500 mV the one-electron processes to attain the other redox states of the ligand. The formation of a ligand-based radical on the Pd(II)-bound *meso*-aryl tripyrrindione is confirmed by spectroelectrochemical and electron paramagnetic resonance (EPR) methods.

## Introduction

Linear oligopyrroles have been known for several decades as naturally occurring and synthetic pigments.¹ Among the tripyrrolic compounds, tripyrranes (in which the pyrrole rings are bridged by methylene groups) are important precursors for the synthesis of porphyrinoid macrocycles,²,³ including texaphyrin-based drug candidates.⁴,⁵ In contrast, conjugated tripyrrins (Fig. 1), with methine bridges between the pyrrole rings, are rather difficult intermediates prone to degradation in the presence of nucleophiles and/or bases.⁶ Nevertheless, the tripyrrin motif, is present in numerous expanded porphyrins² and was recently incorporated in the design of new fluorophores<sup>8,9</sup> and double-helical assemblies.¹0,¹¹¹

Despite the array of pyrrolic nitrogen donors for tridentate binding of metal ions, linear tripyrrins are underutilized in coordination chemistry when compared to tetrapyrrolic and dipyrrolic systems. <sup>12</sup> The limited stability of early tripyrrin compounds featuring methine bridges and all-alkyl substitution of the pyrrole rings likely hindered the broad use of these ligands; however, a number of complexes were reported over the years (Fig. 1a), <sup>13</sup> including several examples of coordination polymers. <sup>14</sup> Interestingly, tripyrrin complexes featuring 5,10-diaryl (aka *meso*-diaryl) substitution (Fig. 1b) were isolated serendipitously following

the oxidative degradation of *N*-confused porphyrins. <sup>15</sup> In fact the ligand in these complexes is tripyrrin-1-one, consistent with the reported tendency of 5,10-diaryl tripyrranes and tripyrrins to oxidize at one of the terminal  $\alpha$  position. <sup>16,17</sup> A *meso*-pentafluorophenyl tripyrrin-1-one was later used for the synthesis of a fluorescent zinc(II) complex (Fig. 1c) and for the detection of zinc by fluorescence microscopy in cultured cells. <sup>18</sup> The gentle oxidation and subsequent metal insertion of *meso*-phenyl tripyrrane with chloranil and Ni(OAc)<sub>2</sub>, respectively, led to a bis(5,10-diphenyl-tripyrrinato) nickel(II) complex of octahedral geometry; however, the tripyrrin intermediate could not be isolated and its oxidative degradation to a black oligomeric material was reported. <sup>19</sup>

Figure 1. The tripyrrin scaffold and examples of tripyrrin ligands and their metal

In recent years, tripyrrin-1,14-dione was identified as a robust

redox-active platform for metal coordination.<sup>20</sup> This biopyrrin motif

shares the scaffold of heme metabolites that were initially isolated

as urinary pigments.<sup>21,22</sup> The β-alkyl substituted tripyrrindione

Department of Chemistry and Biochemistry, The University of Arizona, 1306 E. University Blvd., Tucson, AZ 85721-0041, USA. Email: tomat@arizona.edu

Electronic Supplementary Information (ESI) available: NMR spectroscopic and electrochemical characterization data, details of X-ray diffraction data collection and analysis.

ligands (i.e., H<sub>3</sub>TD1 and H<sub>3</sub>TD2, Fig. 1) coordinate multiple divalent transition metals as stable dianionic radicals (e.g., [Pd(TD1\*)(H<sub>2</sub>O)], Fig. 1).<sup>23–27</sup> Easily accessible one-electron processes in these complexes reversibly alter the redox state of the tripyrrindione ligand. In the case of the Zn(II) complex, the tripyrrindione ligand produced a rare example of fluorescence emission from a radical chromophore.<sup>25</sup> Multi-center interactions between delocalized spins lead to dimers of tripyrrindione radicals in the solid state and at low temperature in solution.<sup>26,28</sup> Although most reported tripyrrindione complexes present an aqua ligand as a monodentate donor within the primary coordination sphere, examples featuring isocyanates<sup>26</sup> and primary amines<sup>27</sup> underscore the ability to modify the properties of this versatile ligand.

Synthetic methods to prepare the naturally occurring biopyrrins have only become available very recently,  $^{29}$  and all tripyrrindione complexes reported to date have featured ethyl or methyl  $\beta$ -substituents on the pyrrole rings (Fig. 1).  $^{30,26}$  Even with this simplified structure, these syntheses required the multi-step preparation of 3,4-dialkyl pyrrole and did not allow for facile, additional functionalization of the ligand scaffold. To further extend the scope of the tripyrrindione ligand system, herein we report the synthesis and palladium(II) coordination of the first 5,10-diaryl-tripyrrin-1,14-dione. In addition, we include comparisons to a new 1,14-dimethoxy-tripyrrin precursor and its palladium complex, which are instructive in the broader context of delineating the chemistry of tripyrrin ligands.

# **Results and Discussion**

#### Synthesis and characterization of ligands

The previously reported tripyrrindione ligands (i.e.,  $H_3TD1$  and  $H_3TD2$ , Fig. 1) were synthesized through condensation of 3,4-diethyl-2,5-diformyl-1*H*-pyrrole and a 3-pyrrolin-2-one precursor (2 equiv) under basic conditions. <sup>26,30</sup> An analogous condensation strategy failed to produce the desired *meso*-aryl tripyrrindione when starting from aroyl diketones or benzylic diols as precursors for the central pyrrole.

The oxidation of 5,10-bis(pentafluorophenyl)-tripyrrane was then pursued using common oxidants such as 2,3-dichloro-5,6-dicyano-1,4-benzoquinone (DDQ), hydrogen peroxide, and peroxycarboxylic acids (e.g., mCPBA). We also tested chloroauric acid, which has been used in the oxidation of *meso*-pentafluorophenyltetrapyrrane to yield three bilindione isomers. These oxidative transformations generally produced tripyrrin-1-one (as previously reported in the case of DDQ)<sup>16</sup> and/or a complex mixture of oligomers. Photooxidation of the tripyrrin-1-one, analogous to the synthesis of dipyrrin-1,9-dione from dipyrrin-1-one,<sup>32,33</sup> also failed to produce the desired product with two terminal pyrrolin-2-one moieties. Recent reports on the use of 1,14-dibromo-5,10-diaryltripyrrins as substrates for nucleophilic substitutions<sup>8,10</sup> prompted us to pursue a synthetic route through this key precursor.

The *meso*-pentafluorophenyl-tripyrrane was synthesized from pyrrole and pentafluorobenzaldehyde under acidic conditions<sup>34,35</sup> and then subjected to bromination with *N*-bromosuccinimide (NBS)

at -78°C and subsequent oxidation with DDQ to afford 5,10-bis(pentafluorophenyl)- $\alpha$ , $\alpha$ '-dibromotripyrrin (HTB<sub>CGF5</sub>, Scheme 1) as previously reported.<sup>8</sup> Next, nucleophilic substitution with sodium methoxide (3.0 equiv) afforded 5,10-bis(pentafluorophenyl)- $\alpha$ , $\alpha$ '-dimethoxy-tripyrrin (HTM<sub>CGF5</sub>, Scheme 1). As previously reported for *meso*-pentafluorophenyl porphyrins<sup>36</sup> and dipyrrins,<sup>37</sup> tripyrrin HTM<sub>CGF5</sub> is susceptible to reactivity with nucleophiles: an excess of sodium methoxide results in additional methoxy substitution at the *para* position of the pentafluorophenyl ring through nucleophilic aromatic substitution.

The new dimethoxytripyrrin ligand  $HTM_{C6F5}$  was purified by chromatography and then precipitated from  $CH_2Cl_2$ /hexane as a red solid. Finally, demethylation of  $HTM_{C6F5}$  with aluminum trichloride in dry  $CH_2Cl_2$  gave the desired 5,10-bis(pentafluorophenyl)-tripyrrin-1,14-dione ( $H_3TD_{C6F5}$ ), which was purified by chromatography and isolated as an orange solid. Given the availability of tripyrrane precursors with a variety of substituents, this synthetic procedure is expected to allow the future preparation of several other tripyrrindione ligands.

Scheme 1. Synthesis of 5,10-di(pentafluorophenyl)-tripyrrin-1,14-dione (H<sub>3</sub>TD<sub>C6FS</sub>)

The  $^1\text{H}$  NMR spectrum of HTM<sub>C6F5</sub> in CDCl<sub>3</sub> at room temperature shows five distinct signals (Fig. S1): three resonances for the pyrrolic  $\beta$ -protons, a broad singlet at 12.89 ppm due to the NH proton, and a sharp tall singlet at 4.17 ppm due to the methoxy protons. The successful conversion to H<sub>3</sub>TD<sub>C6F5</sub> was evident in the  $^1\text{H}$  NMR spectrum of the product (Fig. S2): the methoxy resonances of the starting material disappeared and the tripyrrin NH signal shifted upfield, overlapping with the other NH protons and integrating to three. In the  $^{13}\text{C}$  NMR spectra, the methoxy carbon resonance for the dimethoxytripyrrin is at 57.2 ppm whereas the carbonyl carbon resonance for the tripyrrindione is at 174.8 ppm (Figs. S1-S2).

The small number of resonances for  $H_3TD_{C6F5}$  indicates a symmetrical conformation of the ligand in solution but does not specify the configuration of the double (Z vs. E) and single bonds (syn vs. anti) between adjacent pyrrole rings. NOESY NMR data, however, showed through-space effects only between the  $\beta$ -CH protons of the terminal pyrrolic units and no interactions between the NH and  $\beta$ -CH protons (Fig. S3), therefore indicating a ZZ, syn, syn configuration (as drawn in Scheme 1). In addition, the sharp resonance at 10.8 ppm is

similar to those observed for  $\beta$ -alkyl-substituted tripyrrindiones<sup>30</sup> and dipyrrinones<sup>38</sup> forming hydrogen-bonded dimers in chloroform solutions. This NH signal is broadened into the baseline when collected in an acetone- $d^6$  solution (Fig. S4), consistent with formation of a monomer in a hydrogen-bonding, polar solvent and fast exchange with residual water as we previously observed in the case of H<sub>3</sub>TD1 in methanol.<sup>39</sup> Notably, the pyrrolic NH remains strongly deshielded and clearly visible for HTM<sub>C6F5</sub> in acetone (at ~13 ppm, Fig. S4) owing to the intramolecular hydrogen-bonding interactions with the iminic nitrogen atoms.

Single crystals suitable for X-ray diffraction analysis were obtained by slow diffusion of pentane into solutions of  $HTM_{C6F5}$  or  $H_3TD_{C6F5}$  in  $CH_2Cl_2$ . The crystal structure of the dimethoxytripyrrin (Fig. 2) reveals a nearly planar tripyrrolic scaffold: one of the terminal pyrrole units is only 7.5° out of plane with respect to the other two.

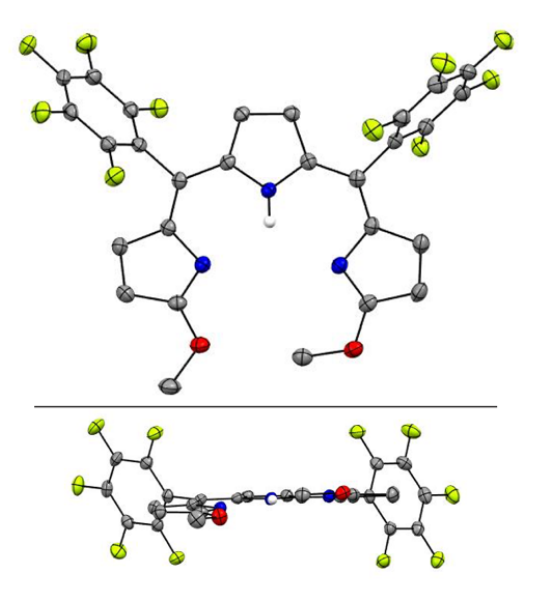


**Figure 2.** Top and side views of the crystal structure of HTM<sub>CGFS</sub>. Carbon-bound hydrogen atoms in calculated positions are omitted for clarity. The pyrrolic nitrogen-bound hydrogen atom was located on the Fourier map during refinement. Non-hydrogen atoms are displayed as thermal ellipsoids set at 50% probability level (CCDC 2300776).

Indeed, the bulky pentafluorophenyl substituents also led to an essentially planar tripyrrin unit in the case of  $\alpha,\alpha'$ -dianilinotripyrrins. <sup>40</sup> Lacking the NH hydrogen-bonding donors of the aniline derivatives, <sup>10,40</sup> however, HTM<sub>C6F5</sub> does not adopt a double helical arrangement. Instead, the HTM<sub>C6F5</sub> ligands pack in a herringbone pattern with pairs of ligands oriented in antiparallel fashion.

The crystal structure of  $H_3TD_{C6F5}$  confirmed the *ZZ*, *syn*, *syn* conformation indicated by the NMR data (Fig. 3a) and revealed a helical dimer featuring two hydrogen-bonding interactions between the lactam units on both ends of the tripyrroles (Fig. 3b,c). This type of intermolecular hydrogen bonding was reported for hexaethyl tripyrrindione  $H_3TD1$ , in which the twisting of the terminal pyrrolinones relative to the plane of the middle pyrrolic unit is about  $20^{\circ}$  on each side. For  $H_3TD_{C6F5}$ , the twisting is asymmetrical, with angles of  $^{\sim}32^{\circ}$  and  $12^{\circ}$  at the aryl-substituted bridges. Both M and P helices, each featuring four hydrogen-bonding interactions (Fig. 3b), are observed in the crystal structure.

The electrochemical profiles of HTM<sub>C6F5</sub> and H<sub>3</sub>TD<sub>C6F5</sub> were investigated by cyclic voltammetry in CH<sub>2</sub>Cl<sub>2</sub> (Fig. S5). The voltammogram of HTM<sub>C6F5</sub> displays one quasi-reversible oxidation event at 0.634 V. Conversely, similar to the hexaethyl tripyrrindione ligand H<sub>3</sub>TD1,<sup>23</sup> H<sub>3</sub>TD<sub>C6F5</sub> has a rather complicated redox profile featuring at least three irreversible oxidations above -0.2 V, which in turn elicit two irreversible reduction events past -1.0 V.

## Synthesis and characterization of palladium(II) complexes

The formation of square planar palladium complexes is well documented for tripyrrins $^{6,41}$  and tripyrrindiones, $^{23,24}$  therefore we sought to investigate the Pd(II) coordination chemistry of both HTM<sub>C6F5</sub> and H<sub>3</sub>TD<sub>C6F5</sub>. The reactions were conducted in the presence of palladium(II) acetate at room temperature (Scheme 2) and monitored by optical absorption spectroscopy (Fig. 4).

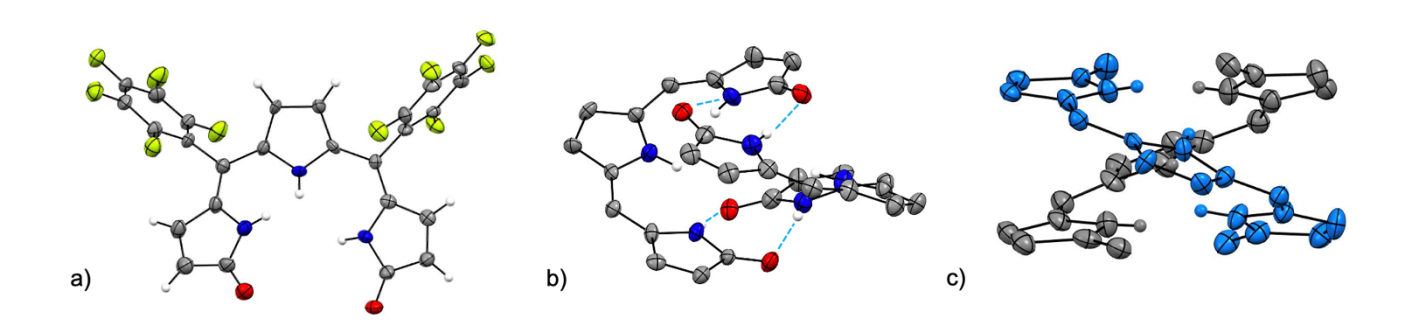
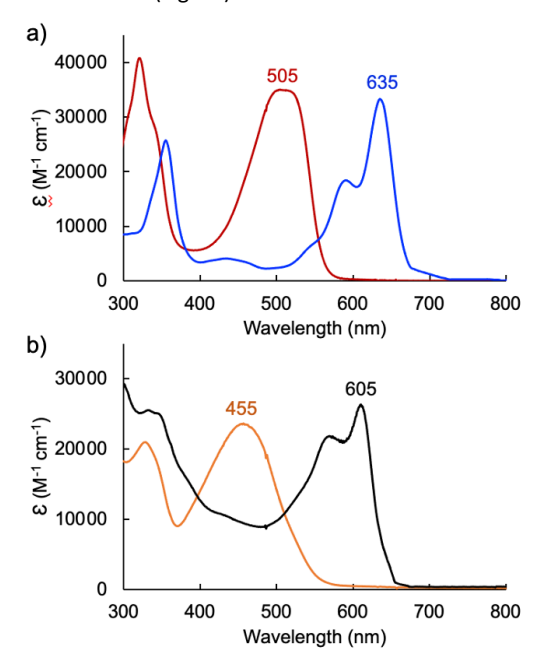


Figure 3. Crystal structure of 5,10-bis(pentafluorophenyl)-tripyrrin-1,14-dione H<sub>3</sub>TD<sub>C6FS</sub>, which crystallizes as a helical dimer. a) Top view, b) side view of the dimer showing four hydrogen bonds as dashed lines, and c) side view of the dimers showing the relative orientation of the two tripyrrolic scaffolds. Carbon-bound hydrogens in calculated positions and aryl substituents are omitted for clarity in the dimer views. Pyrrolic nitrogen-bound hydrogen atoms were located on the Fourier map during refinement. Non-hydrogen atoms are displayed as thermal ellipsoids set at 50% probability level (CCDC 2300775).

Scheme 2. Syntheses of square planar Pd(II) complexes of tripyrrin  $HTM_{CGFS}$  and tripyrrindione  $H_3TD_{CGFS}$ 

In the case of dimethoxytripyrrin HTM<sub>C6F5</sub>, metal coordination led to the appearance of a new peak at 635 nm, causing a color change of the reaction mixture from red to blue. Following purification by column chromatography, initial  $^1$ H NMR data indicated the formation of a complex with an asymmetric tripyrrolic ligand. A total of five peaks were observed in the aromatic region, and a singlet integrating to three protons at 4.13 ppm indicated only one methoxy group in the product (Fig. S6). The structure was ultimately determined through X-ray diffraction analysis (*vide infra*) and showed a square planar cyclometallated Pd(II) complex, resulting from C( $sp^3$ )—H bond activation at one of the methoxy groups. The peak at 6.57 ppm corresponds to the Pd-bound CH<sub>2</sub> protons as determined by  $^1$ H- $^1$ 3C HSQC NMR methods (Fig. S5).



 $C(sp^2)$ –Pd bonds are well-established within the coordination chemistry of *N*-confused porphyrins,<sup>42</sup> carbaporphyrins,<sup>43</sup> and several expanded porphyrins.<sup>44,45</sup> In contrast,  $C(sp^3)$ –Pd bonds, which are relevant to Pd-based organometallic catalysis,<sup>46</sup> are not common for oligopyrrolic ligands. Relevant but distinct examples with polydentate nitrogen ligands include the intramolecular

 $C(sp^3)$ —H bond activation observed in Pd(II) complexes of 6-alkyl-2,2′-bipyridines<sup>47</sup> and t-butyl-substituted 1,3-bis(aryliminio)-isoindolines.<sup>48</sup> Neutral complex [Pd(TM<sub>CGF5</sub>#)] (Scheme 2) therefore represents a unique example of tripyrrin coordinating as a tetradentate dianionic ligand (i.e.,  $(TM_{CGF5}#)^2$ ) through three pyrrolic N donors and one  $C(sp^3)$  donor.

Initial coordination attempts on H<sub>3</sub>TD<sub>C6F5</sub> using Pd(OAc)<sub>2</sub> in THF under ambient conditions proved unsuccessful. Within an hour, the solution color changed from orange to green and a metallic film was observed, indicating slow reduction of the metal cation concurrent with oxidative degradation of the ligand. This observation is in contrast with our previous findings on hexaalkyl tripyrrindiones, which undergo one-electron oxidation in air upon coordinating Pd(II) and other divalent metals as dianionic radicals (e.g., [Pd(TD1\*)(H<sub>2</sub>O)]).<sup>23-27</sup> To facilitate the isolation of a Pd(II) complex of the meso-aryl tripyrrindione in its most reduced state (i.e., TD<sub>C6F5</sub>3-), we added tetra-n-butylammonium bromide (i.e., [(C<sub>4</sub>H<sub>9</sub>)<sub>4</sub>N]Br) to the reaction mixture so as to provide a monocationic counterion soluble in organic solvents. In these conditions, the reaction proceeded steadily, as determined by a color change from orange to blue and consumption of H<sub>3</sub>TD<sub>C6F5</sub> in the absorption profile (Fig. 4b). The spectrum of the complex displays a main absorption band at 605 nm, and no bands were observed at longer wavelengths. The lack of weak intraligand  $\pi\text{-}\pi$  charge transfer bands, which characterize radical tripyrrindione complexes,<sup>23–27</sup> was the first indication of a trianionic binding mode for the isolated complex. <sup>1</sup>H NMR data confirmed the isolation of a diamagnetic species (Fig. S8): three resonances between 5.7 and 6.5 ppm correspond to the  $\beta$ -CH protons, four peaks in the aliphatic regions account for the tetrabutylammonium ion, and the 2H peak at 11.16 ppm was tentatively assigned to a coordinated aqua ligand as found in other tripyrrindione complexes.

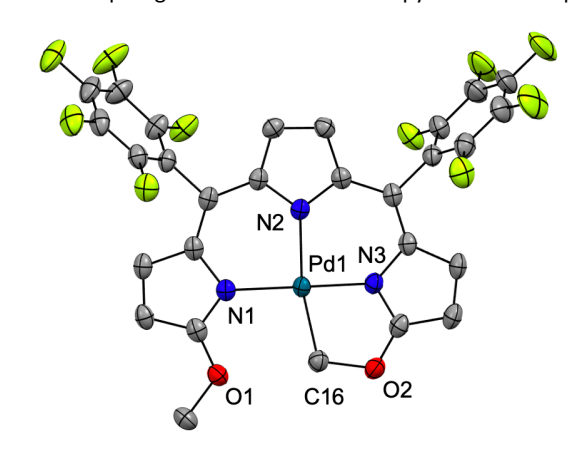


**Figure 5.** Crystal structure of [Pd(TM<sub>CoFs</sub>#)]. Carbon-bound hydrogens in calculated positions are omitted for clarity. Non-hydrogen atoms are displayed as thermal ellipsoids set at 50% probability level (CCDC 2300774).

The crystal structure of [Pd(TM<sub>C6F5</sub>#)] (Figure 5) shows a square planar cyclometallated Pd(II) complex in which a carbon atom from one of the methoxy groups is bound to the Pd(II) center following  $C(sp^3)$ —H activation. The Pd1–C16 bond distance is 2.035 Å, similar to that to the  $C(sp^3)$  donor in the 1,3-bis(aryliminio)isoindoline complexes (2.056 and 2.039 Å).<sup>49</sup> Consistent with a strong *trans* 

influence of the C16 donor, the Pd1–N2 distance to the central pyrrole, which is typically the shorter of the three,  $^{6,23}$  is slightly elongated to 2.067 Å. In contrast, the Pd1–N3 distance is shorter (1.934 Å) because of the formation of the five-membered metallacycle. [Pd(TM<sub>C6F5</sub>#)] packs in a herringbone pattern similar to that of the free ligand and no  $\pi$  stacking is observed.

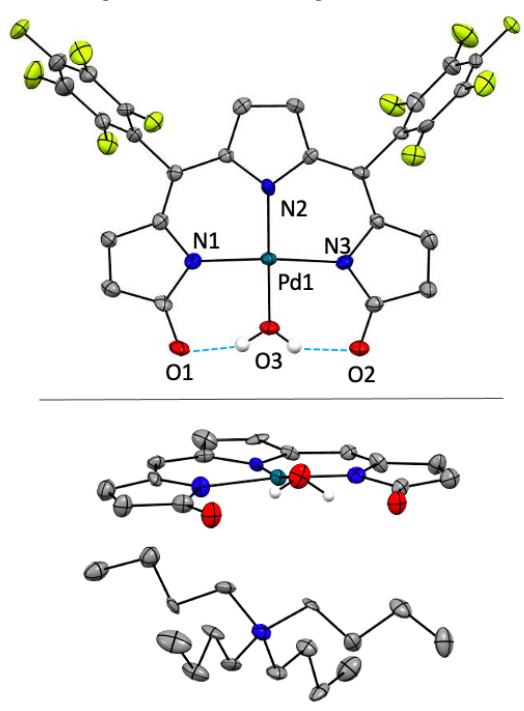


**Figure 6.** Crystal structure of  $[N(C_4H_9)_4][Pd(TD_{C6F_9})(H_2O)]$ . In the top panel, the cation is omitted for clarity. In the bottom panel, the cation is shown whereas the aryl groups are omitted. Carbon-bound hydrogens in calculated positions are omitted for clarity. Non-hydrogen atoms are displayed as thermal ellipsoids set at 50% probability level (CCDC 2300777).

The crystal structure of [TBA][Pd(TD<sub>C6F5</sub>)(H<sub>2</sub>O)] reveals a square Pd(II)-bound tripyrrindione associated tetrabutylammonium ion (i.e., TBA) confirming the anionic nature of the complex (Figure 6). The Pd(II) center also coordinates an aqua ligand, which is engaged in hydrogen-bonding interactions to the carbonyl groups as observed in other tripyrrindione<sup>23,24,26</sup> and dipyrrindione complexes. 50,51 The metal center lies in the plane of the three nitrogen donors while the aqua ligand is 10.3° out of plane. The observed C=O bond lengths (1.269 and 1.249 Å) are comparable to those found in the anionic complex [Pd(TD1)(H<sub>2</sub>O)]<sup>-</sup> (1.260 and 1.259 Å) and longer than those in the neutral radical [Pd(TD1\*)(H<sub>2</sub>O)] (1.240 and 1.238 Å), indicating a similar correspondence between the structural metrics and the ligand redox state.<sup>23</sup> Indeed, the donoracceptor distances for the hydrogen bonds in [Pd(TD<sub>C6F5</sub>)(H<sub>2</sub>O)]<sup>-</sup> (2.534 and 2.528 Å) are also in agreement with those found in [Pd(TD1)(H<sub>2</sub>O)]<sup>-</sup> (2.521 and 2.525 Å), indicative of stronger hydrogen bonds compared to those in neutral and cationic Pd(II) tripyrrindione complexes, which feature longer donor-acceptor distances. No stacking of the tripyrrindione units is observed: instead, the anionic complexes and the tetrabutylammonium cations alternate in a sheet-like packing.

The electrochemical profile of [Pd(TM<sub>C6F5</sub>#)] (Figure 7a, blue trace) presents a wide open-circuit potential window between two one-electron events: a quasi-reversible oxidation at 0.50 V and a quasi-reversible reduction at -1.26 V. There are no reports of the electrochemical profile of cyclometallated Pd(II) tripyrrins; however, the electrochemical profile resembles that of symmetrical tripyrrin complexes, <sup>41</sup> with the first one-electron events assigned as ligand-based and occurring at similar potentials (oxidations occur between 0.36 and 0.45 V, and reductions between -1.01 and -1.37 V).

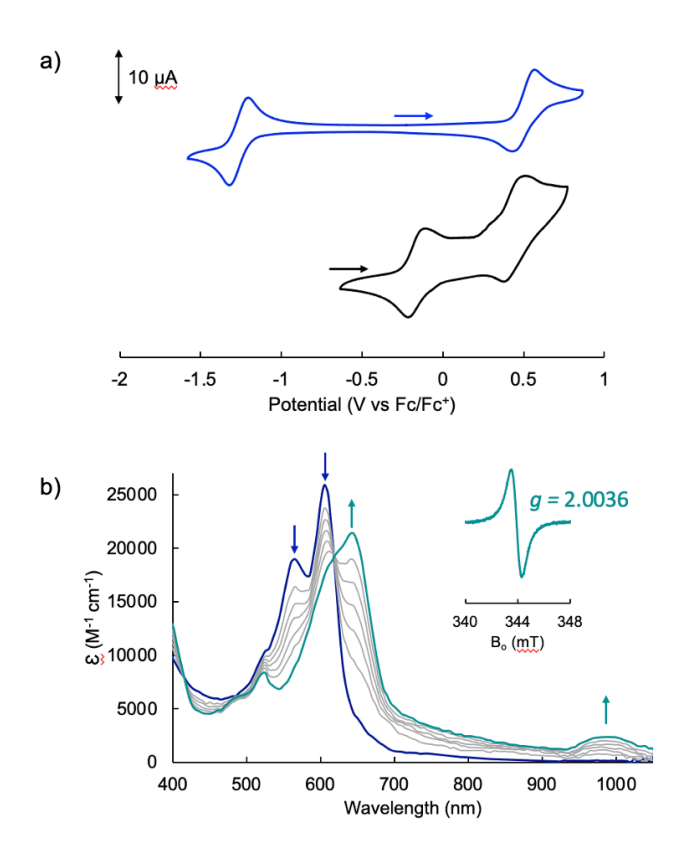


**Figure 7.** Electrochemical analysis of the Pd(II) tripyrrin complexes. a) Cyclic voltammograms of [Pd( $TM_{C6F5}^{*}$ )] (blue trace) and [TBA][Pd( $TD_{C6F5}$ )( $H_2O$ )] (black trace) at a glassy carbon electrode in  $CH_2CI_2$  with 0.1 M [(n-Bu<sub>4</sub>)(PF<sub>6</sub>)] as a supporting electrolyte. Data collected at a 100 mV·s<sup>-1</sup> scan rate using a Ag/AgNO<sub>3</sub> reference electrode and a Pt wire auxiliary electrode. b) Spectral changes observed upon oxidation of [Pd( $TD_{C6F5}$ )( $H_2O$ )]<sup>-</sup> ( $CH_2CI_2$ , 0.1 M (n-Bu<sub>4</sub>)(PF<sub>6</sub>)) by controlled potential electrolysis (at 0.2 V vs. Fc<sup>+</sup>/Fc) to give [Pd( $TD_{C6F5}^{*}$ )( $H_2O$ )]. Inset: EPR spectrum at room temperature of [Pd( $TD_{C6F5}^{*}$ )( $H_2O$ )]; experimental conditions: mw frequency, 9.643 GHz; mw power, 3 mW; field modulation amplitude, 0.05 mT.

The voltammogram of [TBA][Pd( $TD_{C6F5}$ )( $H_2O$ )] (Figure 7a, black trace) presents one quasi-reversible oxidation event at -0.165 V and a second quasi-reversible oxidation at 0.439 V. A small shoulder is observed around 0.33 V and is attributed to partial decomposition upon the first oxidation event. When compared to the ligand-based redox processes of the hexaethyl tripyrrindione complex  $[Pd(TD1^{\bullet})(H_2O)]$ , which is reduced at -0.672 V to form  $[Pd(TD1)(H_2O)]^{-}$  and oxidized at -0.052 V to  $[Pd(TD1)(H_2O)]^{+}$ , it is clear that the *meso*-pentafluorophenyl substitution causes a significant anodic shift (by  $\sim 500$  mV) of the redox profile of the complex. The two one-electron events are assigned as oxidations of

the anionic complex  $[Pd(TD_{C6F5})(H_2O)]^-$  to give the radical  $[Pd(TD_{C6F5}^{\bullet})(H_2O)]$  and then the cation  $[Pd(TD_{C6F5})(H_2O)]^+$ .

We further investigated the first oxidation event of  $[Pd(TD_{C6F5})(H_2O)]^-$  by controlled-potential electrolysis and monitored the progress via spectroelectrochemical methods (Fig. 7b). When the cell potential was held at 0.2 V (vs. Fc/Fc $^+$ ), a decrease in the main absorption bands of  $[Pd(TD_{C6F5})(H_2O)]^-$  (565 and 605 nm) was accompanied by the appearance of a new main absorption band at 633 nm and a long-wavelength band at 990 nm, which is characteristic of metal-bound tripyrrindione radicals.

The formation of a tripyrrindione radical was confirmed through the chemical oxidation of [TBA][Pd(TD<sub>C6F5</sub>)( $H_2O$ )] with silver(I) tetrafluoroborate in acetone. The EPR spectrum of the oxidation product at room temperature (Fig. 7b, inset) resembles that of previously reported tripyrrindione radicals, with a single isotropic line at g = 2.0036 and a width of 0.84 mT. Whereas [Pd(TD1 $^{\bullet}$ )(H<sub>2</sub>O)] forms EPR-silent  $\pi$ -dimers at lower temperatures through multicentered interaction between the ligand-based spins,<sup>28</sup> no loss of EPR signal was observed for [Pd(TD<sub>CGF5</sub>\*)(H<sub>2</sub>O)] at 77 K (Fig. S9). Differences in the spin distribution on the ligand scaffold as well as the effect of the bulky aryl substituent are likely decreasing the ability of the complexes to engage in pancake bonding. Although  $[Pd(TD_{C6F5}^{\bullet})(H_2O)]$  is fairly stable in solution at room temperature (Fig. S10), when attempting to isolate or crystallize this complex we observed a tendency to demetalate and/or oligomerize at high concentrations leading to an intractable solid. Further investigations on the effects of meso-aryl substituents on the stability of tripyrrindione radical complexes are underway.

# **Experimental**

# Materials and methods

The synthesis of meso-di(pentafluorophenyl)tripyrrane<sup>35</sup> and HTB<sub>C6F5</sub><sup>52</sup> were performed according to reported procedures. Dichloromethane (CH2Cl2), pentane and THF were dried by passage through a solvent purifier. Dry solvents were confirmed to contain <0.1 ppm H<sub>2</sub>O using a Mettler Toledo C10S Coulometric Karl Fisher Titrator. All other commercial reagents were used without further purification. Aluminum-backed silica gel plates (thickness: 200 µm) were used to monitor reactions by thin layer chromatography (TLC). Chromatographic purifications on silica gel were conducted on a Biotage Isolera One Flash instrument. <sup>1</sup>H, <sup>13</sup>C and <sup>19</sup>F NMR spectra were recorded on a Bruker NEO-500 instrument at the NMR Facility of the University of Arizona (UArizona) Department of Chemistry and Biochemistry. UV-visible absorption spectra were obtained at ambient temperature using an Agilent 8453 spectrophotometer or an Agilent Cary 60 spectrophotometer. High-resolution mass spectrometry data were acquired at the UArizona Mass Spectrometry Core Facility. Elemental analyses were performed by Numega Resonance Labs, San Diego, CA. The continuous-wave (CW) EPR experiments were carried out at the UArizona Department of Chemistry and Biochemistry EPR facility on an X-band Elexsys E500 spectrometer (Bruker Biospin) equipped with a rectangular TE102 resonator.

#### Synthetic procedures

meso-pentafluorophenyl  $\alpha,\alpha'$ -dimethoxytripyrrin (HTM<sub>C6F5</sub>).  $\alpha,\alpha'$ -dibromo-meso-di(pentafluorophenyl)tripyrrin (10 mg, 0.014 mmol) was dissolved in CH<sub>2</sub>Cl<sub>2</sub> (5 mL) and sodium methoxide (2.3 mg, 0.042 mmol) in MeOH (1 mL)) was added. The reaction mixture was stirred at room temperature until the starting material was consumed as determined by TLC. The reaction mixture was then diluted with CH2Cl2 (20 mL) and washed with brine (20 mL). The organic layer was dried over anhydrous Na<sub>2</sub>SO<sub>4</sub> and the crude product was purified by column chromatography on silica gel using CH2Cl2/hexane as eluent. The product was then redissolved and precipitated from CH<sub>2</sub>Cl<sub>2</sub>/hexane to yield a red-orange solid (5.6 mg, 65% yield). <sup>1</sup>H NMR (500 MHz, CDCl<sub>3</sub>):  $\delta$  12.89 (br. s, 1H), 6.66 (d, J = 4.7 Hz, 2H), 6.35 (d, J = 4.7 Hz, 2H), 6.11 (d, J = 2.4 Hz, 2H), 4.17 (s, 6H). <sup>13</sup>C NMR (125 MHz, CDCl<sub>3</sub>): 177.82, 148.8, 136.4, 135.4, 120.6, 117.7, 114.9, 57.2.  $^{19}$ F NMR (470 MHz, CDCl<sub>3</sub>):  $\delta$  -138.09, -152.60, -161.07. UV-vis (CH<sub>2</sub>Cl<sub>2</sub>)  $\lambda_{max}$  ( $\epsilon$ ): 320 (38,000), 505 (35,000). HRMS-ESI<sup>+</sup>:  $[M+H]^+$  calcd. for  $[C_{28}H_{13}F_{10}N_3O_2]$ , 614.09209; found, 614.09207.

meso-pentafluorophenyl tripyrrindione (H3TDc6F5). HTMc6F5 (55 mg, 0.09 mmol) was dissolved in dry CH<sub>2</sub>Cl<sub>2</sub> (20 mL0 under an argon atmosphere, and sodium iodide (161.3 mg, 1.08 mmol) and aluminum trichloride (72 mg, 0.54 mmol) were added at room temperature. The reaction mixture was stirred until the starting material was no longer detected by TLC. Purification of the solution by column chromatography on silica gel with CH<sub>2</sub>Cl<sub>2</sub>/CH<sub>3</sub>OH and precipitation from CH<sub>2</sub>Cl<sub>2</sub>/hexane yielded the desired product as an orange solid (43.7 mg, 73% yield). <sup>1</sup>H NMR (500 MHz, CDCl<sub>3</sub>):  $\delta$  10.77 (br., 3H), 6.73 (d, J = 5.5 Hz, 2H), 6.13 (d, J = 2.0 Hz, 2H), 6.07 (d, J = 5.5 Hz, 2H). <sup>13</sup>C NMR (125) MHz, CDCl<sub>3</sub>): 174.8, 137.0, 136.7, 133.2, 124.5, 116.7, 104.3. <sup>19</sup>F NMR (470 MHz, CDCl<sub>3</sub>):  $\delta$  -138.03, -151.69, -160.61. UV-vis  $(CH_2Cl_2)$   $\lambda_{max}$  ( $\epsilon$ ): 265 (22,400), 328 (20,900), 455 (23,500). HRMS-ESI<sup>+</sup>: [M+H]<sup>+</sup> calcd. for  $[C_{26}H_9F_{10}N_3O_2]$ , 586.06078; found, 586.06086.

[Pd(TM<sub>C6F5</sub> $^*$ )]. Pd(OAc)<sub>2</sub> (1.5 mg, 0.0066 mmol) was added to a solution of  $HTM_{C6F5}$  (3.7 mg, 0.0060 mmol) in  $CH_2Cl_2$  (5 mL) and the reaction was stirred for 3 h. Upon completion, as monitored by UV-visible spectroscopy, the complex was purified by column chromatography using CH<sub>2</sub>Cl<sub>2</sub> as the eluent. The fraction was concentrated down to a blue solid (2 mg, 46 % yield). <sup>1</sup>H NMR  $(500 \text{ MHz}, \text{CDCl}_3)$ :  $\delta$  6.78 (d, J = 5.0 Hz, 2H), 6.57 (s, 2H), 6.47 (d, J = 5.1 Hz, 1H), 6.39 (d, J = 5.0 Hz, 1H), 6.33 (s, 2 H), 4.13 (s, 3 H). <sup>13</sup>C NMR (125 MHz, CDCl<sub>3</sub>): 178.7, 174.9, 142.5, 138.8, 136.8, 135.6, 135.5, 134.4, 123.8, 122.0, 115.3, 108.7, 93.2, 58.5. <sup>19</sup>F NMR (470 MHz, CDCl<sub>3</sub>):  $\delta$  -137.82, -138.45 -152.40, -152.68 -160.98, -161.16. UV-vis (CH<sub>2</sub>Cl<sub>2</sub>)  $\lambda_{max}$  ( $\epsilon$ ): 355 (26,000), 433 (4,700), 590 (18,600), 635 (33,300). HRMS-ESI+: [M+H]+ calcd. for  $[C_{28}H_{11}F_{10}N_3O_2Pd]$ , 717.98099; found, 717.98022. Anal. Calcd. for  $[C_{28}H_{11}F_{10}N_3O_2Pd]$ : C, 46.9; H, 1.5; N, 5.9%; found: C, 47.2; H, 2.1; N, 5.8%.

**[TBA][Pd(TD**<sub>C6F5</sub>)( $H_2O$ )].  $H_3TD$ <sub>C6F5</sub> (4.2 mg, 0.007 mmol) was dissolved in THF (5 mL) and tetra-n-butylammonium bromide (2.8 mg, 0.0086 mmol) was added along with a few drops of CH<sub>3</sub>OH to fully solubilize the salt.  $Pd(OAc)_2$  (1.9 mg, 0.0086

mmol) was then added, and the reaction mixture was stirred under ambient conditions as its color gradually turned from orange to dark blue. The coordination was monitored by optical absorption spectroscopy. Upon completion, the solvent was removed under reduced pressure and the product was crystallized from acetone/hexane as a dark blue solid (4.5 mg, 66% yield). <sup>1</sup>H NMR (CDCl<sub>3</sub>):  $\delta$  = 11.16 (br, 2 H), 6.43 (d, 2H, J= 5.2 Hz), 6.04 (d, 2H, J = 5.2 Hz), 5.75 (s, 2H), 3.28 (t, 8 H, J = 8.9Hz), 1.59 (m, 8 H), 1.31 (m, 8H), 0.89 (t, 12 H, J = 7.2 Hz) ppm. <sup>13</sup>C NMR (125 MHz, CDCl<sub>3</sub>): 211.2, 166.6, 160.8, 142.2, 141.9, 132.8, 58.8, 24.1, 19.7, 13.7. <sup>19</sup>F NMR (470 MHz, CDCl<sub>3</sub>):  $\delta$  = -139.6, -154.5, -162.1. UV-vis (CH<sub>2</sub>Cl<sub>2</sub>)  $\lambda_{max}$  ( $\epsilon$ ): 344 (24,100), 565 (21,600), 605 (25,900). HRMS-ESI<sup>-</sup>: [M]<sup>-</sup> calcd. for  $[C_{26}H_8F_{10}N_3O_3Pd]$ , 705.94463; found, 705.94427. Anal. Calcd. for  $[C_{42}H_{44}F_{10}N_4O_4Pd] \bullet CH_2Cl_2 \bullet 1.5(H_2O)$ : C, 48.7; H, 4.7; N, 5.3%; found: C, 48.8; H, 5.1; N, 5.2%.

#### **Electrochemical measurements**

Cyclic voltammograms were performed on a Gamry Reference 600 potentiostat utilizing a single-compartment cell with three electrodes: a glassy carbon working electrode, a platinum wire auxiliary electrode, and a Ag/AgCl reference electrode. Measurements were performed at ambient temperature under an inert argon atmosphere in  $CH_2Cl_2$  containing 0.1 M [( $n-Bu_4N$ )(PF<sub>6</sub>)] (triply recrystallized) as a supporting electrolyte. Sample concentrations were 1–2 mM, and all electrochemical data were internally referenced to the ferrocene/ferrocenium couple (set at 0.00 V).

## Chemical oxidation of [Pd(TD<sub>C6F5</sub>)(H<sub>2</sub>O)]<sup>-</sup> and EPR analysis

Due to the limited stability of  $[Pd(TD_{C6F5}^{\bullet})(H_2O)]$  upon solvent removal, this species was formed in situ and analyzed as such. A sample of  $[Pd(TD_{C6F5})(H_2O)]^-$  (1 mM in acetone) was oxidized with AgBF<sub>4</sub> (1.1 equiv). The sample was filtered through a celite plug to remove elemental silver. An aliquot (0.5 mL) was taken and diluted by half with toluene for analysis both at room temperature and 77 K.

## Conclusions

We report the synthesis and characterization of the first examples of two new classes of tripyrrolic ligands featuring *meso*-pentafluorophenyl substituents, namely 1,14-dimethoxytripyrrin HTM<sub>C6F5</sub> and tripyrrin-1,14-dione H<sub>3</sub>TD<sub>C6F5</sub>. The synthetic route from a tripyrrane precursor is expected to allow for a variety of *meso*-aryl groups. Additionally, the reactivity at the *para* positions of the pentafluorophenyl substituents<sup>36,37</sup> will allow for post-synthetic functionalization of HTM<sub>C6F5</sub> and H<sub>3</sub>TD<sub>C6F5</sub> and their further utilization as building blocks.

Both of the prepared tripyrroles coordinate Pd(II) at ambient temperature to form square planar complexes. HTM<sub>C6F5</sub> undergoes  $C(sp^3)$ —H bond activation in the presence of palladium(II) acetate leading to the formation of the cyclometallated complex [Pd(TM<sub>C6F5</sub>#)], in which the ligand binds in a dianionic tetradentate fashion including a Pdmethylene bond. In contrast, tripyrrindione H<sub>3</sub>TD<sub>C6F5</sub> binds

Pd(II) as a trianionic ligand and the resulting complex  $[TBA][Pd(TD_{C6F5})(H_2O)]$  features an aqua ligand and a tetrabutylammonium counterion.

The *meso*-aryl substituents changed substantially the electrochemical profile of the tripyrrindione ligand: whereas hexaalkyl tripyrrindiones coordinate divalent cations as dianionic radicals (i.e., TD1°2- or TD2°2-) under aerobic conditions, this *meso*-pentafluorophenyl analog stabilizes complexes in the most reduced state of the ligand (i.e., TD<sub>C6F5</sub>3-). Spectroelectrochemical and EPR spectroscopic experiments confirmed that the radical state of the novel *meso*-pentafluorophenyl tripyrrindione complex remains accessible upon one-electron oxidation at –0.165 V (vs Fc/Fc<sup>+</sup>). Notably, the shifted redox profile of the new *meso*-aryl tripyrrindione could accommodate coordination of metal cations of higher oxidation states, which have not been previously explored for this class of pyrrolic ligands.

Modifications of the aryl substituents and associated electronic effects are expected to modulate the coordination chemistry of these ligands as well as the electronic structure<sup>53</sup> and reactivity of the complexes, including C—H bond activation chemistry and one-electron redox processes. The optical and/or electrochemical properties of these tripyrrinato complexes could prove advantageous in applications in photocatalysis<sup>54</sup> and energy conversion and storage,<sup>55</sup> including in redox flow batteries requiring wide open-circuit potential windows as observed here for [Pd(TM<sub>CGF5</sub>#)]. Furthermore, inspired by the well-established supramolecular chemistry of *meso*-aryl porphyrins,<sup>56,57</sup> *meso*-diaryl tripyrrin and tripyrrindione complexes could serve as new redox-responsive building blocks for supramolecular assemblies, with additional tunability provided by the monodentate ligand at the fourth coordination site.

### **Conflicts of interest**

There are no conflicts to declare.

# **Acknowledgements**

We thank Dr. Vlad Kumirov, Dr. William Montfort, and Dr. Andrei Astashkin for assistance with the acquisition and analysis of NMR, X-ray diffractometry, and EPR data, respectively. This work was supported by the National Science Foundation (award CHE-2203361 to E.T.). The Bruker NEO-500 spectrometer and the Bruker D8 Venture diffractometer in the UArizona Dept. of Chemistry and Biochemistry NMR Facility and X-ray Diffraction Facility, respectively, were purchased thanks to support from the National Science Foundation (MRI awards CHE-1920234 and CHE-2117516).

# **Notes and references**

1 H. Falk, *The Chemistry of Linear Oligopyrroles and Bile Pigments*, Springer-Verlag, Vienna, 1989.

- 2 J. L. Sessler and D. Seidel, Synthetic Expanded Porphyrin Chemistry, *Angew. Chem. Int. Ed.*, 2003, **42**, 5134–5175.
- 3 T. Tanaka and A. Osuka, Chemistry of meso-Aryl-Substituted Expanded Porphyrins: Aromaticity and Molecular Twist, *Chem. Rev.*, 2017, **117**, 2584–2640.
- 4 J. F. Arambula and J. L. Sessler, Porphyrinoid Drug Conjugates, *Chem*, 2020, **6**, 1634–1651.
- 5 G.-Q. Jin, C. V. Chau, J. F. Arambula, S. Gao, J. L. Sessler and J.-L. Zhang, Lanthanide porphyrinoids as molecular theranostics, Chem. Soc. Rev., 2022, 51, 6177–6209.
- 6 M. Bröring and C. D. Brandt, Tripyrrin—the missing link in the series of oligopyrrolic ligands, Chem. Commun., 2001, 499–500.
- 7 J. L. Sessler and S. J. Weghorn, Expanded, Contracted, and Isomeric Porphyrins; Pergamon Press: New York, 1997.
- 8 J.-F. Wang, Y. Yao, Y. Ning, Y.-S. Meng, C.-L. Hou, J. Zhang and J.-L. Zhang, The design of rigid cyclic tripyrrins: the importance of intermolecular interactions on aggregation and luminescence, *Org. Chem. Front.*, 2018, 5, 1877–1885.
- 9 Y. Yao, C.-L. Hou, Z.-S. Yang, G. Ran, L. Kang, C. Li, W. Zhang, J. Zhang and J.-L. Zhang, Unusual near infrared (NIR) fluorescent palladium(II) macrocyclic complexes containing M—C bonds with bioimaging capability, *Chem. Sci.*, 2019, 10, 10170–10178.
- 10 M. Umetani, T. Tanaka and A. Osuka, Conjugated double helices *via* self-dimerization of  $\alpha$ , $\alpha'$ -dianilinotripyrrins, *Chem. Sci.*, 2018, **9**, 6853–6859.
- 11 K. Ueta, M. Umetani, A. Osuka, G. D. Pantoş and T. Tanaka, Singleand double-helices of  $\alpha$ , $\alpha'$ -dibenzylaminotripyrrin: solution and solid state studies, *Chem. Commun.*, 2021, **57**, 2617–2620.
- 12 E. Tomat, Coordination Chemistry of Linear Tripyrroles: Promises and Perils, *Comments Inorg. Chem.*, 2016, **36**, 327–342.
- 13 M. Bröring, in *Handbook of Porphyrin Science*, World Scientific Publishing Company, 2010, vol. 8, pp. 343–501.
- 14 M. Bröring, S. Prikhodovski, C. D. Brandt and E. Cónsul Tejero, Pillars, Layers, Pores and Networks from Nickeltripyrrins: A Porphyrin Fragment as a Versatile Building Block for the Construction of Supramolecular Assemblies, *Chem. Eur. J.*, 2007, 13, 396–406.
- 15 H. Furuta, H. Maeda and A. Osuka, Regioselective Oxidative Liberation of Aryl-Substituted Tripyrrinone Metal Complexes from N-Confused Porphyrin, Org. Lett., 2002, 4, 181–184.
- 16 J.-Y. Shin, S. S. Hepperle, B. O. Patrick and D. Dolphin, Oxidized forms of a tripyrrane: α-tripyrrinone, β-tripyrrinone and a C2 symmetric hexapyrrole, *Chem. Commun.*, 2009, 2323.
- 17 M. Gałeęzowski, J. Jaźwiński, J. P. Lewtak and D. T. Gryko, Rational Synthesis of Tripyrranes, *J. Org. Chem.*, 2009, **74**, 5610–5613.
- 18 Y. Ding, Y. Xie, X. Li, J. P. Hill, W. Zhang and W. Zhu, Selective and sensitive "turn-on" fluorescent Zn<sup>2+</sup> sensors based on di- and tripyrrins with readily modulated emission wavelengths, *Chem. Commun.*, 2011, **47**, 5431–5433.
- 19 P. P. Liu, Y. Q. Feng, C. Z. Gu, C. J. Li, S. X. Meng and B. Zhang, A Meso-Substituted Tripyrrin Metal Complex as the Candidate for Fluorescent Material, Adv. Mat. Res., 2012, 557–559, 665–668.
- 20 E. Tomat and C. J. Curtis, Biopyrrin Pigments: From Heme Metabolites to Redox-Active Ligands and Luminescent Radicals, Acc. Chem. Res., 2021, 54, 4584–4594.
- 21 J. Beruter, J.-P. Colombo and U. P. Schlunegger, Isolation and Identification of the Urinary Pigment Uroerythrin, *Eur. J. Biochem.*, 1975, **56**, 239–244.
- 22 T. Yamaguchi, I. Shioji, A. Sugimoto, Y. Komoda and H. Nakajima, Chemical Structure of a New Family of Bile Pigments from Human Urine, *J. Biochem.*, 1994, **116**, 298–303.

- 23 R. Gautam, J. J. Loughrey, A. V. Astashkin, J. Shearer and E. Tomat, Tripyrrindione as a Redox-Active Ligand: Palladium(II) Coordination in Three Redox States, *Angew. Chem. Int. Ed.*, 2015, 54, 14894–14897.
- 24 S. Bahnmüller, J. Plotzitzka, D. Baabe, B. Cordes, D. Menzel, K. Schartz, P. Schweyen, R. Wicht and M. Bröring, Hexaethyltripyrrindione (H3Et6tpd): A Non-Innocent Ligand Forming Stable Radical Complexes with Divalent Transition-Metal Ions, Eur. J. Inorg. Chem., 2016, 8.
- 25 R. Gautam, S. J. Petritis, A. V. Astashkin and E. Tomat, Paramagnetism and Fluorescence of Zinc(II) Tripyrrindione: A Luminescent Radical Based on a Redox-Active Biopyrrin, *Inorg. Chem.*, 2018, 57, 15240–15246.
- 26 E. Tomat, C. J. Curtis, A. V. Astashkin, J. Conradie and A. Ghosh, Multicenter interactions and ligand field effects in platinum( ιι ) tripyrrindione radicals, *Dalton Trans.*, 2023, 52, 6559–6568.
- 27 I. Habenšus, A. Ghavam, C. J. Curtis, A. V. Astashkin and E. Tomat, Primary amines as ligands and linkers in complexes of tripyrrindione radicals, *J. Porphyrins Phthalocyanines*, 2023, 27, 1448–1456.
- 28 R. Gautam, A. V. Astashkin, T. M. Chang, J. Shearer and E. Tomat, Interactions of Metal-Based and Ligand-Based Electronic Spins in Neutral Tripyrrindione  $\pi$  Dimers, *Inorg. Chem.*, 2017, **56**, 6755–6762.
- 29 T. Mujawar, P. Sevelda, D. Madea, P. Klán and J. Švenda, A Platform for the Synthesis of Oxidation Products of Bilirubin, J. Am. Chem. Soc., 2024, 146, 1603–1611.
- S. D. Roth, T. Shkindel and D. A. Lightner, Intermolecularly hydrogen-bonded dimeric helices: tripyrrindiones, *Tetrahedron*, 2007, 63, 11030–11039.
- 31 J.-F. Wang, F. Ma, H.-L. Sun, J. Zhang and J.-L. Zhang, Three bilindione isomers: synthesis, characterization and reactivity of biliverdin analogs, *J. Biol. Inorg. Chem.*, 2017, **22**, 727–737.
- 32 E. Tomat, Propentdyopents: Brief history of a family of dipyrrolic pigments, *J. Porphyrins Phthalocyanines*, 2019, **23**, 1265–1272.
- 33 R. Bonnett, S. Ioannou and F. J. Swanson, Propentdyopents and related compounds. Part 4. Propentdyopent—alkanol adducts by the photo-oxygenation of pyrromethenones, *J. Chem. Soc., Perkin Trans.* 1, 1989, 711–714.
- 34 C. Brückner, E. D. Sternberg, R. W. Boyle and D. Dolphin, 5,10-Diphenyltripyrrane, a useful building block for the synthesis of meso-phenyl substituted expanded macrocycles, *Chem. Commun.*, 1997, 1689–1890.
- 35 J.-W. Ka and C.-H. Lee, Optimizing the synthesis of 5,10-disubstituted tripyrromethanes, *Tetrahedron Lett.*, 2000, **41**, 4609–4613.
- 36 J. I. T. Costa, A. C. Tomé, M. G. P. M. S. Neves and J. A. S. Cavaleiro, 5,10,15,20-tetrakis(pentafluorophenyl)porphyrin: a versatile platform to novel porphyrinic materials, *J. Porphyrins Phthalocyanines*, 2011, **15**, 1116–1133.
- 37 H. R. A. Golf, H.-U. Reissig and A. Wiehe, Nucleophilic Substitution on (Pentafluorophenyl)dipyrromethane: A New Route to Building Blocks for Functionalized BODIPYs and Tetrapyrroles, *Org. Lett.*, 2015, **17**, 982–985.
- 38 M. T. Huggins and D. A. Lightner, Hydrogen-Bonded Dimers in Dipyrrinones and Acyldipyrrinones, *Monatsh. Chem.*, 2001, 132, 203–221.
- 39 A. Swain, B. Cho, R. Gautam, C. J. Curtis, E. Tomat and V. Huxter, Ultrafast Dynamics of Tripyrrindiones in Solution Mediated by Hydrogen-Bonding Interactions, J. Phys. Chem. B, 2019, 123, 5524–5535.

- 40 A. Nishiyama, K. Ueta, M. Umetani, Y. Akamatsu and T. Tanaka, Substituent Effects at the 5,10-Positions of Dianilinotripyrrins on Their Dimerization Themodynamics, *Chem. Asian J.*, 2022, **17**, e202200562.
- 41 J. Bley-Escrich, S. Prikhodovski, C. D. Brandt, M. Bröring and J.-P. Gisselbrecht, Electrochemical investigations of tripyrrin complexes, *J. Porphyrins Phthalocyanines*, 2003, **07**, 220–226.
- 42 M. Toganoh and H. Furuta, Creation from Confusion and Fusion in the Porphyrin World—The Last Three Decades of N-Confused Porphyrinoid Chemistry, *Chem. Rev.*, 2022, **122**, 8313–8437.
- 43 T. D. Lash, Carbaporphyrinoid Systems, *Chem. Rev.*, 2017, **117**, 2313–2446.
- 44 S. Mori, S. Shimizu, R. Taniguchi and A. Osuka, Group 10 Metal Complexes of *meso*-Aryl-Substituted [26]Hexaphyrins with a Metal–Carbon Bond, *Inorg. Chem.*, 2005, **44**, 4127–4129.
- 45 T. Yoneda, Y. M. Sung, J. M. Lim, D. Kim and A. Osuka, Pd <sup>II</sup> Complexes of [44]- and [46]Decaphyrins: The Largest Hückel Aromatic and Antiaromatic, and Möbius Aromatic Macrocycles, *Angew. Chem. Int. Ed.*, 2014, **53**, 13169–13173.
- 46 G. C. Dickmu and I. P. Smoliakova, Cyclopalladated complexes containing an (sp³)C–Pd bond, *Coord. Chem. Rev.*, 2020, **409**, 213203.
- 47 A. Zucca, M. A. Cinellu, M. V. Pinna, S. Stoccoro, G. Minghetti, M. Manassero and M. Sansoni, Cyclopalladation of 6-Substituted-2,2'-bipyridines. Metalation of Unactivated Methyl Groups vs Aromatic C–H Activation, Organometallics, 2000, 19, 4295–4304.
- 48 M. Bröring and C. Kleeberg, Facile intramolecular C(sp3)—H bond activation with PdII, *Chem. Commun.*, 2008, 2777.
- 49 C. Kleeberg and M. Bröring, Palladium complexes of unsymmetrical 1,3-bis(aryliminio)isoindoline (BAI) ligands: A novel class of complexes exhibiting unusual structural features, *Polyhedron*, 2010, **29**, 507–513.
- 50 C. J. Curtis and E. Tomat, Heteroleptic palladium(II) complexes of dipyrrin-1,9-dione supported by intramolecular hydrogen bonding, *J. Porphyrins Phthalocyanines*, 2020, **24**, 112–120.
- 51 C. J. Curtis, A. V. Astashkin, J. Conradie, A. Ghosh and E. Tomat, Ligand-Centered Triplet Diradical Supported by a Binuclear Palladium(II) Dipyrrindione, *Inorg. Chem.*, 2021, 60, 12457– 12466.
- 52 C.-L. Hou, Y. Yao, D. Wang, J. Zhang and J.-L. Zhang, Orthogonally arranged tripyrrin–BODIPY conjugates with an "edge to plane" mode, *Org. Chem. Front.*, 2019, **6**, 2266–2274.
- 53 A. Kumar, B. Thompson, R. Gautam, E. Tomat and V. Huxter, Temperature-Dependent Spin-Driven Dimerization Determines the Ultrafast Dynamics of a Copper(II)-Bound Tripyrrindione Radical, *J. Phys. Chem. Lett.*, 2023, 11268–11273.
- 54 R. Costa E Silva, L. Oliveira Da Silva, A. De Andrade Bartolomeu, T. J. Brocksom and K. T. De Oliveira, Recent applications of porphyrins as photocatalysts in organic synthesis: batch and continuous flow approaches, *Beilstein J. Org. Chem.*, 2020, 16, 917–955.
- 55 J. Min Park, J. H. Lee and W.-D. Jang, Applications of porphyrins in emerging energy conversion technologies, *Coord. Chem. Rev.*, 2020, **407**, 213157.
- 56 C. M. Drain, A. Varotto and I. Radivojevic, Self-Organized Porphyrinic Materials, *Chem. Rev.*, 2009, **109**, 1630–1658.
- 57 S. Durot, J. Taesch and V. Heitz, Multiporphyrinic Cages: Architectures and Functions, Chem. Rev., 2014, 114, 8542–8578.